X-692-75-177
PREPRINT

BOW SHOCK AND MAGNETOSHEATH WAVES AT MERCURY

D. H. FAIRFIELD
K. W. BEHANNON

JULY 1975

GODDARD SPACE FLIGHT CENTER
GREENBELT, MARYLAND

BOW SHOCK AND MAGNETOSHEATH WAVES AT MERCURY

D.H. Fairfield and K.W. Behannon
Laboratory for Extraterrestrial Physics
NASA/Goddard Space Flight Center
Greenbelt, Maryland

ABSTRACT

Mariner 10 measurements at the Mercury bow shock provide examples where the magnetic field is approximately parallel or perpendicular to the bow shock normal. Upstream of a broad irregular parallel shock, left hand circularly polarized waves are observed which cut off very sharply at~4 Hz. Upstream of a perpendicular shock, right hand circularly polarized waves are observed which persist up to the Nyquist frequency of 12 Hz. Determination of the wave propagation vector as a function of frequency helps conclusively identify the waves as whistler mode waves propagating from the shock. The magnetosheath downstream of the parallel shock is disturbed more than that downstream of the perpendicular shock particularly below 1 Hz. In the latter case regular left hand polarized waves observed slightly above the proton gyrofrequency are identified as ion cyclotron waves with wavelength~300 km which have been doppler shifted up to their observed frequency.

Introduction

Bow shock waves have been detected upstream from the planets Earth (Ness et al., 1964), Venus (Bridge et al., 1967; Dolginov et al., 1968), Mars (Bogdanov and Vaisberg, 1975), Jupiter (Smith et al., 1974), and Mercury (Ness et al., 1974b). The extensive studies carried out near Earth reveal the bow shock as a relatively thin (usually less than a few proton gyroradii) surface separating the upstream region of relatively quiet conditions from a downstream region of higher magnitude, fluctuating magnetic fields and higher density, hot shocked plasmas. The thickness and structure of the shock is determined by the upstream mach number (Greenstadt et al., 1975; Fairfield and Feldman, 1975), the plasma β ($\beta = \frac{nk_B(T_e + T_p)}{B^2/8\pi}$ where n is the plasma density, k_B the Boltzman constant, T_e and T_p the electron and proton temperatures and B the field strength) (Formisano et al., 1975), and the relative orientation of the upstream magnetic field and the shock normal (Greenstadt et al., 1970; Greenstadt, 1972).

When the field is within approximately 40° of the shock surface, the shock transition is well defined and relatively thin (Greenstadt et al., 1970; Fairfield, 1974). When this angle is greater than 40° the transition is complex and extends over a region many thousands of kilometers thick in which irregular large amplitude waves occur

(Greenstadt et al., 1970). In the latter case, low frequency waves are frequently observed to persist many 10's of R_E (Earth Radii) into the upstream region (Fairfield, 1969). Such waves typically have periods 20-60 sec, polarizations that are generally left-handed, and amplitudes which often approach that of the total field. Such waves are thought to be generated in the upstream region by particles emanating from the shock (Fairfield, 1969; Barnes, 1970; and Fredricks, 1975). Higher frequency waves with periods near 2.5 sec are sometimes seen in packets (Russell et al., 1971) which are usually associated with the lower frequency waves.

Continuous upstream waveforms with frequencies of 0.5-4 Hz (Fairfield, 1974) are observed within a few minutes of most shock crossings and occasionally persist for much longer times. These waves are seen with either left or right-hand polarization and with amplitudes of $\frac{\Delta B}{B} \approx 1$. The left-hand polarized waves tend to cutoff sharply at a frequency generally not exceeding 2.5 Hz, whereas the right-hand waves persist to higher frequencies. The waves usually have their propagation direction $\hat{k}$ oriented at an angle of 20^{o}-40^{o} from the field direction, $\vec{B}$, and the sense of polarization is determined by the propagation direction or, alternatively by the field direction. The observations are adequately explained as right-hand polarized whistler waves

propagating from the shock into the upstream region. When $\vec{k}$ has a large component antiparallel to the solar wind velocity, $\vec{V}$, the waves are doppler-shifted, the phase velocity is reversed in the spacecraft frame of reference and the waves are observed to be left-handed.

The magnetic field downstream from the shock in the magnetosheath (Fairfield, 1975) is the solar wind magnetic field which has been convected through the bow shock. At the shock, the field undergoes a compression and the acute angle change necessary to preserve the normal component across the shock. Convection within the magnetosheath further distorts the field until it is aligned approximately tangent to the magnetopause near that boundary. A complex variety of waves are superposed on the average field, but little progress has been made in identifying specific wave modes and the locations where the waves are generated. Average spectra vary as $1/f$ below the proton gyrofrequency and $1/f^3$ above it, but peaks appear at different times and at different frequencies. The more highly fluctuating magnetic fields tend to be associated with the irregular parallel shocks (Formisano, et al. 1973) and may be due to convection of the low frequency (T = 20-60 sec) upstream waves into the magnetosheath (Fairfield and Ness, 1970).

The present paper extends the initial analysis of Mariner 10 observations of the bow shock and magnetosheath of Mercury taken on March 29, 1974. Mariner 10, the only spacecraft to encounter this

planet, made an additional pass on the anti-sun side of the planet on March 16, 1975. These more recent data confirm the earlier observations of an intrinsic planetary field and provide additional bow shock observations which support the data tc be discussed below. The data from the initial encounter provide an outstanding example of different types of shock structures and of upstream whistler propagation. The identification of wave modes is made particularly clear through the application of recent advances in spectral analysis techniques which yield the wave propagation direction as a function of frequency. Such techniques are also used to provide the first identification of ion cyclotron waves in a planetary magnetosheath.

Data

The complete set of Mercury magnetic field observations taken on March 29, 1974 is shown in figure 1 (Ness et al., 1974b). The trajectories of the spacecraft past the planet on March 29, 1974 and also on March 16, 1975 are shown in figure 2. On March 29 the spacecraft, moving at a velocity of 11 km/sec relative to the planet, first encountered the bow shock at 20h27m10s. The shock moved in past the spacecraft at 20h27m30s and the spacecraft again penetrated the shock at 20h27m57s. Mariner 10 traversed the dusk magnetosheath (MS) in 9 minutes, crossed the magnetopause at 20h36m59s and passed behind the planet where it measured a planetary magnetic field (Ness et al., 1974b, 1975). The spacecraft emerged from the magnetosphere at 20h54m12s, crossed the

dawn magnetosheath in 3 minutes and encountered a thick poorly-defined shock where the field magnitude decreased over the interval 20h57m20s-20h59m10s. During the last minute of this interval, irregular low frequency (T~5-10 sec) waves of indeterminate polarization were present which may well be similar to the low frequency waves seen at Earth. Superposed on these low frequency waves and persisting beyond them were higher frequency waves which are discussed in detail below. A final brief encounter with the shock occured at 21h00m10s. (See Ness et al., 1974b figures 4 and 5 for detail data plots of both inbound and outbound shocks).

The rapidity of this traversal approximates a more "instantaneous" picture of the planetary-solar wind interaction than is possible with a single spacecraft at the Earth or other large planets with extended magnetospheres. We note that the interplanetary field just prior to the initial shock encounter is only about 30° different in direction from the average field when the spacecraft emerges from the outbound shock 33 minutes later.

The trajectories in figure 2 are indicated by dashed lines with the boundary crossings designated by dots or heavy lines. The solid curves in figure 2 represent the average bow shock and magnetopause locations determined at the Earth (Fairfield, 1971), which have been scaled for Mercury by equating the 11.0 R_E magnetopause distance at Earth to a 1.3 R_M

(Mercury Radii) standoff distance at Mercury (Whang and Ness, 1975). Choosing an alternate Mercury standoff distance of 1.6 (Ness et al., 1975; Whang and Ness, 1975) moves the crossing point relative to the boundaries to a distance 17% closer to the planetary center. Although the 1.3 value appears to give better agreement, the uncertainties associated with interplanetary conditions at Mercury (density $n = 17 \pm 2$ cm^{-3}, velocity $V = 630 \pm 40$ km/sec at $3^{\circ} \pm 6^{\circ}$ west of the sun on March 29, 1974 (Ogilvie et al., 1974)) relative to average conditions at the Earth mean that this is not a precise method for determination of the subsolar distance.

Normals to the model shock were calculated at the location of the observed shock. The inbound normal ($\hat{n}$ = (.607, .739, -.292) was only 3° different from that estimated by Ness et al. (1974b) who used the average field ahead of the first crossing and after the third crossing and assumed that $\vec{B}$ was perpendicular to $\hat{n}$. This agreement confirms the fact that the inbound shock is very nearly a perpendicular shock. More specifically, the average field for ten seconds ahead of the first shock crossing made an angle of 90° with the model normal and the average field between the shocks made an angle of 80° with the normal. The outbound model normal ($\hat{n}$ = (.557,-.813,.170)) makes an angle

of 15° with the field direction during the minutes that low frequency waves are present, but an angle close to 40° during subsequent intervals when they are absent. This behavior is reminiscent of field direction control of low frequency waves observed at Earth's bow shock.

Spectral Analysis

The power spectrum analysis used in this study was performed using the mean-lagged-product method of Blackman and Tukey (1958). In this method the power spectral estimates are computed from finite Fourier transforms of the autocorrelation functions of time series consisting of each orthogonal magnetic field component and the field magnitude. Any slow trends in the component or magnitude data are removed by subtracting a second degree polynomial fit to the data.

In addition to computation of power spectral density estimates for the field components and magnitude, coherence and phase functions are also computed using standard definitions (Bendat and Piersol, 1971). A further stage of the analysis is the computation of eigenvalues and eigenvectors by diagonalization of the real symmetric part of the spectral matrix using a Givens-Householder technique (Wilkenson, 1965). The resulting eigenvalues represent the power densities in the directions of maximum, intermediate and minimum fluctuation of the magnetic field. The associated directions are given by the eigenvectors. The eigenvector associated with the minimum eigenvalue may be interpreted

as the wave normal direction, k , and the full spectral matrix rotated to a coordinate system where this direction is the new Z-axis (Means, 1972; McPherron et al., 1972). In this new coordinate system a plane wave analysis for polarization parameters can be performed (Fowler et al., 1967; Rankin and Kurtz, 1970).

Another "wave normal vector" is independently computed using a second method suggested by Means (1972), which uses only the imaginary part of the spectral matrix. Close agreement between this and the previously obtained wave normal vector is taken as an indicator of the reliability of the wave normal determination in terms of low interference from unwanted signals. Note that Means' method breaks down for linear polarization.

For each of the two Mercury encounter periods the magnetic field experiment was commanded into a fixed high range, automatic bias mode of operation (see Ness et al., 1974a for a description of experiment instrumentation). In the high range ($\pm$ 128γ) the digitization noise level for spectral studies is $4 \times 10^{-4}\ \gamma^2/\text{Hz}$.

IV. Upstream Waves

One prominent feature of the Mercury encounter data is the observation of waves with frequencies > .5 Hz upstream from and adjacent to both inbound and outbound shock crossings. Power spectra were calculated for the interval between the latter two of the three inbound shock crossings and for three representative outbound intervals, all

of which are designated by bars in figures 1 and 2. The three outbound spectra were very similar in all respects and are represented by the 21h 00m 25s - 21h 00m 50s spectra shown in the upper right portion of figure 3. Spectra from between the inbound shocks are shown in the upper left. In both cases z is the average field direction over the interval and x and y are transverse to the field direction with x in the solar ecliptic xz plane. Similar waves were seen for a ten second interval preceding the initial inbound shock crossing.

The inbound upstream waves were right-hand polarized, and appreciable power was observed up to the Nyquist frequency of 12.5 Hz. The outbound waves were left-hand polarized, and power decreased to the instrumental noise level between 3 and 4.5 Hz. A correction for instrumental attenuation (down 3 db at 5 Hz) was not applied to the date of figure 3 but would have the effect of making the inbound spectra flatter while not appreciably changing the character of the outbound spectra. The spectral slopes associated with each polarization are similar to those seen for similar waves at the Earth (Fairfield, 1974).

Below each set of spectra in figure 3 are the solar ecliptic components of the minimum variance direction $\hat{k}$, the angle α between the solar wind direction (approximated by the mercury-sun line) and $\hat{k}$, the angle θ between $\hat{k}$ and $\vec{B}$, and the angle δ between the minimum variance

direction determined using the two methods. The inbound right-hand waves propagate in a direction that is relatively independent of frequency. This direction has a large southward component, and α is between 60° and 90° and θ between 40° and 60° in the frequency range below 7 Hz where $\hat{k}$ is determined most accurately. The left-handed waves between 1.0 and 2.5 Hz propagate primarily in the upstream direction with $\alpha \approx 35^\circ$ and $\theta \approx 20^\circ$. Above 2.5 Hz θ increases gradually with increasing frequency up to 4.3 Hz where the spectra approach the instrumental digitization noise level and $\hat{k}$ is not meaningful. The directions of $\hat{k}$ and $\hat{B}$ are shown schematically in figure 2 where these vectors have been rotated into the plane of the figure about $\hat{X}$ and $\hat{k}$ in order to preserve the approximate α and θ.

To explain these observations we apply the cold plasma dispersion relation for whistlers above the ion gyrofrequency:

$$c^2k^2/\omega' = \omega^2_{pe}/(\omega' - \Omega_e \cos\theta) \qquad (1)$$

where c is the speed of light, k is the magnitude of the wave propagation vector, ω' is the plasma frame frequency, $\omega^2_{pe} = \frac{4\pi ne^2}{m_e}$ is the electron plasma frequency with e the electronic charge and m_e the electron mass, and $\Omega_e = \frac{eB}{m_e c}$ is the electron gyrofrequency with m_e the mass of the electron. We must also consider that the measured frequency, ω, is related to the plasma frame frequency of (1) by

where $V_{ph} = \omega/k$ is the phase velocity. In order to propagate upstream, waves must have the component of their group velocity parallel to the outward pointing shock normal greater than the component of the solar wind velocity anti-parallel to the normal. We plot this parallel component of the group velocity in the top portions of figure 4 for the various θ values. The dash-dot lines delineate the possible extremes of the component of solar wind velocity along the shock normal where the range of values is determined by the $\pm$ 40 km/sec uncertainty in the measured solar wind velocity and the $\pm 6^{\circ}$ uncertainty in the direction. In the outbound case it is clear that waves with $k \geq .04$ to .1 (depending on the extremes of solar wind velocity and θ) can propagate upstream. Waves with $\theta = 2^{\circ}$ and k's of .05 to .1 ($\lambda = \frac{2\pi}{k}$ of $\sim$ 125 - 60 km) will indeed be seen with left-hand polarizations (i.e. negative frequencies) up to frequencies of 2.5 Hz. Waves with larger θ's can be seen at higher left hand frequencies (i.e. more negative frequencies) and hence are in agreement with the observations of figure 3 which show higher θ's between 3 at 4.5 Hz. The theory explains the cutoff frequency of left-hand waves as a limit to the amount of doppler shift. This limit does not apply to the right-hand waves which are observed at higher frequencies. We conclude that the whistlers propagating upstream from the dawn sector Mercury bow shock that are observed at frequencies between 1 and 4 Hz with left-hand polarization are in fact right-hand polarized

in the plasma frame, with plasma frame frequencies between approximately 2 and 8 Hz and wavelengths between about 60 and 130 km. These frequencies can be compared with the proton gyrofrequency of 0.3 Hz and lower hybrid frequency of 13.0 Hz and lengths $\frac{c}{\omega_{pe}} = 1.3$ km and $\frac{c}{\omega_{pi}} = 55.2$ km. In the inbound case, waves have more difficulty getting upstream because their group velocity makes a large angle to the shock normal. Figure 4 shows that only waves with $K \geq .1$ ($\lambda \leq 60$ km) and plasma frame frequencies > 4 Hz can propagate upstream. These waves will indeed be seen with right-hand polarizations (positive frequencies). Again the cold plasma whistler theory is adequate to explain the observations. During the March 16, 1975 encounter, waves were again seen upstream from the Mercury bow shock. On both inbound and outbound passes, highly coherent left-hand polarized whistler type waves were observed. These waves cut off sharply at frequencies of several Hz, and were propagating with $10^{\circ} \leq \theta \leq 50^{\circ}$ and $10^{\circ} \leq \alpha \leq 40^{\circ}$. These results are entirely consistent with the earlier Mercury and Earth results, although somewhat more elliptical polarization was observed during the 1975 encounter. The 1975 data also revealed the occasional appearance of low frequency waves ($T \simeq 5 - 10$ sec), but their polarization was not well defined. These waves occurred only when the field made an angle of less than 50° with the shock normal and hence are similar to the low frequency waves seen at Earth.

The analytical alternative to constructing figure 4 is to solve the cubic equation obtained from equations 1 and 2 by eliminating ω'. Using measured values for n, ν, θ, ω and α, solutions for k can be obtained for each measured frequency. When applied to the outbound case in figures 3 and 4, this technique yielded the real values of k between .01 and .1 but in addition gave an imaginary part for measured frequencies > 1.9 Hz which was initially small and gradually increased with frequency. This imaginary term can be interpreted as the damping decrement producing the high frequency cutoff, but experimental uncertainties make its value somewhat uncertain.

We further note that waves above 12 Hz are probably necessary to explain the waves observed near 8 Hz inbound (although at high frequencies the $\hat{k}$ direction changes so that the doppler shift term becomes smaller and in fact may change sign [see $\alpha > 90^{\circ}$ in figure 3]), yet in the outbound case, plasma frame frequencies much greater than 12 Hz are not present or else they would be observed as right-hand waves at high frequencies. The reason for this difference is presumably due to the shock structure and the means by which the waves are produced.

Magnetosheath Waves

Data from the disturbed magnetosheath behind the poorly defined outbound shock and the relatively quiet magnetosheath behind the inbound shock are illustrated by the power spectra of the solar ecliptic X component of the field in figure 5. Averages over 1.2 second periods were used to

calculate spectral estimates below 0.42 Hz for the intervals 20h28m0s - 20h32m30s and 20h54m25s - 20h57m12s. Measurements made every 40 milliseconds in the 20 and 25 second intervals adjacent to the shocks were used to calculate the higher frequency spectra. The discontinuity in the inbound spectra (dashed line) at 0.42 Hz is due to enhancement of waves during the short interval near the shock relative to the longer magnetosheath interval represented by the low frequency spectra. The enhancement in power near 1.5 Hz relative to that at 0.4 Hz is, however, persistent throughout the inbound magnetosheath and is the feature of primary interest in this paper.

Figure 6 shows the spectra for the 20 second interval adjacent to the inbound shock. Three components in a field aligned coordinate system are shown along with the quantities defined in figure 3. In figure 6 and for other spectra taken in the inbound magnetosheath, there exists a frequency range (denoted by the vertical dashed lines in figure 6) of highly coherent left-hand polarized waves propagating at a small angle to the field. At slightly lower frequencies and primarily near the shock, waves propagate at a large angle to the field. Above the band of left-handed waves the coherency of the waves deteriorates and the various quantities in figure 6 are probably not meaningful.

Spectra for four other intervals in the inbound magnetosheath are shown in figure 7. Their locations in time and space are indicated by

bars in figures 1 and 2. The Z spectra on the right correspond to the average field direction, and they generally have less power than the X spectra on the left which correspond to a direction perpendicular to the field. The frequency bands of the highly coherent left-hand polarized waves are indicated by the bars at the top of the figure. In all cases these coherent waves are slightly above the proton gyrofrequency, which is indicated by the vertical arrows. The frequency range of the coherent waves moves to lower frequency as the gyrofrequency decreases.

The proximity of these coherent waves to the proton gyrofrequency and their behavior relative to it suggest that the waves might be ion cyclotron waves. Waves of this mode (Stix, 1962, p. 34) have frequencies just below the proton gyrofrequency and the mode undergoes a cutoff at this frequency. For propagation nearly along the field direction, such waves are left-hand circularly polarized when their frequency is near the gyrofrequency, but they become more elliptical at lower frequencies. The question, then, is whether ion cyclotron waves can be doppler-shifted to the higher observed frequencies. The doppler shift term $(\vec{k} \cdot \vec{V})$ could be calculated from measurements except for the fact that the measured direction is ambiguous by a factor of 180° and $|\vec{k}|$ is not measured at all. The cold plasma theory of ion cyclotron waves indicates that $V_{ph} = \omega/k \rightarrow 0$ as $\omega \rightarrow \Omega_p$. The approximately circular polarization of the observed waves suggests that ω is near Ω_p implying that the k is very

large and the doppler shift is large and not well determined. However, for propagation parallel to the field in a finite temperature, plasma there is a maximum value to $|\vec{k}|$ given by Stix (1962, p. 196 eq 27) as

$$|k|^3 < \frac{\pi^{1/2}\,\Omega_p\,\omega^2_{pi}}{c^2}\left(\frac{m_p}{2k_B T_{\parallel}}\right)^{1/2}$$

where $\omega^2_{pi} = \frac{4\pi n e^2}{m_p}$ and $T_{\parallel}$ is the proton temperature parallel to the magnetic field. All quantities needed to evaluate the right-hand side of this equation are measured except $T_{\parallel}$. This latter quantity can be evaluated by using the measured velocity (which should not change appreciably between the Earth and Mercury) and calculating T from the T-V relation of Burlaga and Ogilvie (1973). This gives an interplanetary temperature at 1 AU which can be extrapolated to Mercury at .46 AU using figure 3.8 of Hundhausen (1972), yielding a value of 4×10^5 °K. We then multiply by a factor of 15 to account for the magnetosheath increase in temperature (e.g. Spreiter, et al., 1966) giving 6×10^5 °K as a reasonable value to use for evaluation purposes. Since $|k| \sim T_{\parallel}^{1/6}$, the value is not critical. We determine the magnetosheath velocity in km/sec to be $\vec{V} = 504$ (-.87, .47, -.16) km/sec by multiplying the measured interplanetary value of 630 by .8 to account for a magnetosheath decrease (e.g. Spreiter et al., 1966) and assuming cylindrical

symmetry and flow at a direction 30° from the X axis.

Using this maximum theoretical value for $|k|$ along with the measured values of $\hat{k}$ and the deduced value for $\vec{V}$ we may calculate the doppler shift and compare measurements and theory. Table 1 gives measured and calculated quantities for each of the five intervals of spectral calculations in the inbound magnetosheath. When the $\hat{k}$ vectors varied within the coherent frequency band, two extreme values are given. For each time interval the sum of the plasma frame wave frequency (taken to be $\nu_p = \Omega_{p/2\pi}$) and the calculated doppler shift falls within or very near the range of observed frequencies. The fact that this agreement is achieved with $\vec{k} \cdot \vec{V}$ positive implies that k is oriented in the downstream direction.

In the light of this agreement between theory and measurement we conclude that ion cyclotron waves are an important component in the relatively quiet magnetosheath downstream from an approximately perpendicular shock at Mercury. Although such waves have not been reported in the Earth's magnetosheath, they are undoubtedly present there also.

SUMMARY AND CONCLUSIONS

Measurements at the Mercury bow shock provide outstanding examples of parallel and perpendicular collisionless shocks. As in the case of the Earth's bow shock, low frequency waves ($T \sim 5$-10 sec.) are associated with the more parallel alignment of the upstream field and the shock normal.

Higher frequency (> 1 Hz) waves are found to exhibit a sharp cutoff at 2-4 hz when they are observed to be left-hand polarized; whereas, they persist to higher frequencies when they are observed to be right-hand polarized. The wave propagation direction is determined by diagnalization of the spectral matrix and this information is used to demonstrate that the waves are right-hand polarized whistler mode waves which are doppler-shifted and observed as left-hand polarized when the propagation direction has a large component in the upstream direction. Comparison with cold plasma theory reveals that the waves have plasma frame frequencies of the order of the lower hybrid frequency and wavelengths of the order c/ω_p.

The magnetosheath field downstream from a parallel shock is very irregular and contains considerably more power at frequencies below 1 Hz than that behind a perpendicular shock. In the latter case, however, a highly coherent band of left hand circularly polarized waves is observed

at approximately three times the proton gyrofrequency. By using measured parameters and a theoretical estimate of the wavelength, it is concluded that the observed waves are ion cylotron waves with frequencies just below the ion gyrofrequency which are propagating in the downstream direction and have been doppler-shifted up to their observed frequency. Although this is the first report of ion cylotron waves in a planetary magnetosheath, there appears to be no reason that similar waves should not also be present in the Earth's magnetosheath.

ACKNOWLEDGEMENTS

We wish to acknowledge the use of preliminary measurements from the Mariner 10 Plasma Science Experiment in this investigation. In addition, we appreciate discussions of these results with Drs. N.F. Ness, Y.C. Whang and J.D. Scudder. The contributions of D.R. Howell, F.W. Ottens and P. Harrison to the analysis and processing of the Mariner 10 magnetometer data are also greatly appreciated.

TABLE 1

$\lambda = \frac{2\pi}{k}$

	B(γ)	n	$\hat{k}_x$	$\hat{k}_y$	$\hat{k}_z$	θ	k	(Km)	ν_p	$\vec{V}\cdot\vec{k}$	$\nu_p + \vec{V}\cdot\vec{k}$	Measured ν
20:27.58 - 28.18	44.4	25	-.37	-.17	-.91	10^o-20^o	.023	278	.68	.7	1.4	1.4-2.6
			-.82	.10	-.56					1.5	1.5	
28.38 - 29.03	45.3	25	-.61	.19	-.77	5^o-30^o	.023	276	.69	1.4	2.1	1.4-3.8
			-.83	.04	-.55					1.5	2.2	
30.00 - 30.25	36.9	25	-.91	.19	-.37	10^o-20^o	.021	296	.56	1.6	2.2	1.3-2.8
			-.74	.52	-.43					1.6		
31.35 - 32.00	31.1	25	-.84	.35	-.42	10^o-30^o	.020	313	.48	1.5	2.0	.9-1.9 Hz
			-.98	.11	-.17					1.5		
34.00 - 34.25	39.6	22	-.81	.35	-.47	5^o-15^o	.019	332	.45	1.4	1.8	.6-1.6
			-.92	.11	-.37					1.4		

REFERENCES

Barnes, A., Theory of generation of bow-shock-associated hydromagnetic waves in the upstream interplanetary medium, Cosmic Electrodynamics, 1, 90-114, 1970.

Bendat, J.S. and A.G. Piersol, Random data: analysis and measurement procedures, John Wiley and Sons, New York, 1971 p. 32.

Blackman, R.B. and J.W. Tukey, The Measurement of Power Spectra, Dover, New York, 1958.

Bogdanov, A.V., and O.L. Vaisberg, Structure and variations of solar wind-Mars interaction region, J. Geophys. Res., 80 487-494, 1975.

Bridge, H.S., A.J. Lazarus, C.W. Snyder, E.J. Smith, L. Davis Jr., P.J. Coleman, Jr., and D.E. Jones, Mariner V: Plasma and magnetic fields observed near Venus, Science, 158, 1669-1673, 1967.

Burlaga, L.F. and K.W. Ogilvie, Solar wind temperature and speed, J. Geophys. Res., 78, 2028-2034, 1973.

Dolginov, S.S., E.G. Yeroshenko, and L.N. Zhuzgov, Magnetic field investigations with AIS "Venera-4", Kosmich. Issled, 6, 561-575, 1968 (in Russian)

Fairfield, D.H., Bow shock associated waves observed in the far upstream interplanetary medium, J. Geophys. Res., 74, 3541-3553, 1969.

Fairfield, Donald H., Average and Unusual Locations of the Earths magnetopause and bow shock, J. Geophys. Res., 76, 6700-6716, 1971.

Fairfield, D.H., Whistler waves upstream from collisionless shocks, J. Geophys. Res., 79, 1368-1378, 1974.

Fairfield, D.H., Magnetic field of the magnetosheath, Submitted to Rev. Geophys. and Space Phys., 1975.

Fairfield, D.H. and W.C. Feldman, Standing waves at low Mach number laminar bow shocks, J. Geophys. Res., 80, 515-522, 1975.

Fairfield, D.H., and N.F. Ness, Magnetic field fluctuations in the Earth's magnetosheath, J. Geophys. Res., 75, 6050-6060, 1970.

Formisano, V., G. Moreno and F. Palmiotto, Solar wind interaction with the Earths magnetic field 1. Magnetosheath, J. Geophys. Res., 78, 3714-3730, 1973.

Formisano, V., C.T. Russell, J.D. Means, E.W. Greenstadt, F.L. Scarf and M. Neugebauer, Collisionless shock waves in space: A very high β structure, J. Geophys. Res., 80, 2013-2022, 1975.

Fowler, R.A., B.J. Kotick, and R.D. Elliot, Polarization analysis of natural and artificially induced geomagnetic micropulsations, J. Geophys. Res., 72, 2871-2883, 1967.

Fredricks, R.W., A model for generation of bow-shock-associated upstream waves, J. Geophys. Res., 80, 7-17, 1975.

Greenstadt, E.W., Observation of nonuniform structure of the Earth's bow shock correlated with interplanetary field orientation, J. Geophys. Res., 77, 1729-1738, 1972.

Greenstadt, E.W., I.M. Green, G.T. Inouye, D.S. Colburn, J.H. Binsack, and E.F. Lyon, Dual satellite observations of Earth's bow shock I: the thick pulsation shock, Cosmic Electrodynamics, 1, 160-177, 1970.

Greenstadt, E.W., C.T. Russell, F.L. Scarf, V. Formisano and M. Neugebauer, Structure of the quasi-perpendicular laminar bow shock, J. Geophys. Res., 80, 502-514, 1975.

Hundhausen, A.J., Coronal expansion and solar wind, Springer-Verlag, New York, 1972.

Means, Joseph D., Use of the three-dimensional covariance matrix in analyzing the polarization properties of plane waves, J. Geophys. Res., 77, 5551-5559,1972.

McPherron, R.L., C.T. Russell, and P.J. Coleman, Fluctuating magnetic fields in the magnetosphere, 2. ULF waves, Space Sci. Revs., 13, 411-454, 1972.

Ness, N.F., C. S. Scearce, and J.B. Seek, Initial results of the IMP 1 magnetic field experiment, J. Geophys. Res., 69, 3531-3569, 1964.

Ness, N.F., K.W. Behannon, R.P. Lepping, Y.C. Whang and K.H. Schatten, Magnetic Field Observations Near Venus: Preliminary Results from Mariner 10, Science, 183, 1301-1306, 1974a.

Ness, N.F., K.W. Behannon, R.P. Lepping, Y.C. Whang, K.H. Schatten, Magnetic field observations near Mercury: Preliminary results from Mariner 10, Science, 185, 151-160, 1974b.

Ness, N.F., K.W. Behannon, R.P. Lepping, Y.C. Whang, The magnetic field of Mercury: Part 1, J. Geophys. Res., 80, 2708-2716, 1975.

Ogilvie, K.W., J.D. Scudder, R.E. Hartle, H.S. Bridge, A.J. Lazarus, J.R. Asbridge, S.J. Bame, C.M. Yeates, Observations at Mercury encounter by the plasma science experiment on Mariner 10, Science, 185, 145-151, 1974.

Rankin, D. and R. Kurtz, Statistical study of micropulsation polarizations, J. Geophys. Res., 75, 5444-5458, 1970.

Russell, C.T., D.D. Childers, and P.J. Coleman, Jr., OGO 5 observations of upstream waves in the interplanetary medium: Discrete wave packets, J. Geophys. Res., 76, 845-861, 1971.

Smith, E.J., L. Davis, Jr., D.E. Jones, D.S. Colburn, P.J. Coleman Jr., P. Dyal and C.P. Sonett, Magnetic field of Jupiter and its interaction with the solar wind, Science, 183, 305-306, 1974.

Spreiter, John R., Audrey L. Summers and Alberta Y. Alksne, A field model for the interaction of the solar wind and the geomagnetic field, in Radiation Trapped in the Earth's Magnetic Field, edited by Billy H. McCormac, D. Reidel Publishing Company, Dordrecht Holland, Gordan and Breach, New York, 1966.

Stix, T.H., The Theory of Plasma Waves, McGraw-Hill, New York, 1962.

Whang, Y.C. and N.F. Ness, Modelling the Magnetosphere of Mercury, NASA-GSFC Preprint X-690-75-89, April 1975.

Wilkinson, J.H., The algebraic eigenvalue problem, Clarendon Press-Oxford, 1965.

FIGURE CAPTIONS

Figure 1. Magnetic field magnitude $\bar{F}$, latitude angle θ and longitude angle ϕ shown for the first pass of Mariner 10 past Mercury. 6 second averages are plotted in ME coordinates along with root-mean-square deviation during the averaging interval. (ME = Mercury ecliptic).

Figure 2. Trajectories of Mariner 10 past Mercury on March 29, 1974 and March 16, 1975. Average boundaries are those determined for the Earth which have been scaled for Mercury assuming at 1.3 R_M subsolar distance for the magnetopause.

Figure 3. Power spectra for whistler mode waves observed on the inbound and outbound passes with right-hand and left-hand polarization, respectively. Also shown are the components of the wave vector direction $\hat{k}$, and the angle between both $\hat{k}$ and the solar wind direction (α) and $\hat{k}$ and the upstream field direction, θ. δ is the angular difference between $\hat{k}$ determined from the real and imaginary parts of the spectral matrix.

Figure 4. Plasma frame wave frequency from the cold plasma whistler dispersion relation (solid curves for positive ν) is added to the doppler shift (solid lines at negative ν) to give the observed frequency (dashed curves) as a function of k.

Theoretical group velocities (solid curves at top) lying above the component of the solar wind velocity along the shock normal (dashed lines at top) indicate whistler waves are able to propagate upstream.

Figure 5. Power spectra calculated for the solar ecliptic X component of the field in the inbound and outboard magnetosheath.

Figure 6. Magnetosheath power spectra adjacent to the shock are shown along with the quantities defined in figure 3. A band of highly coherent left-hand circularly polarized waves is indicated by the dashed lines.

Figure 7. Power spectra computed for four 25 second intervals spaced throughout the inbound magnetosheath. The bands of coherent waves indicated by the bars move to lower frequencies as the proton gyrofrequency (vertical arrows) decreases.

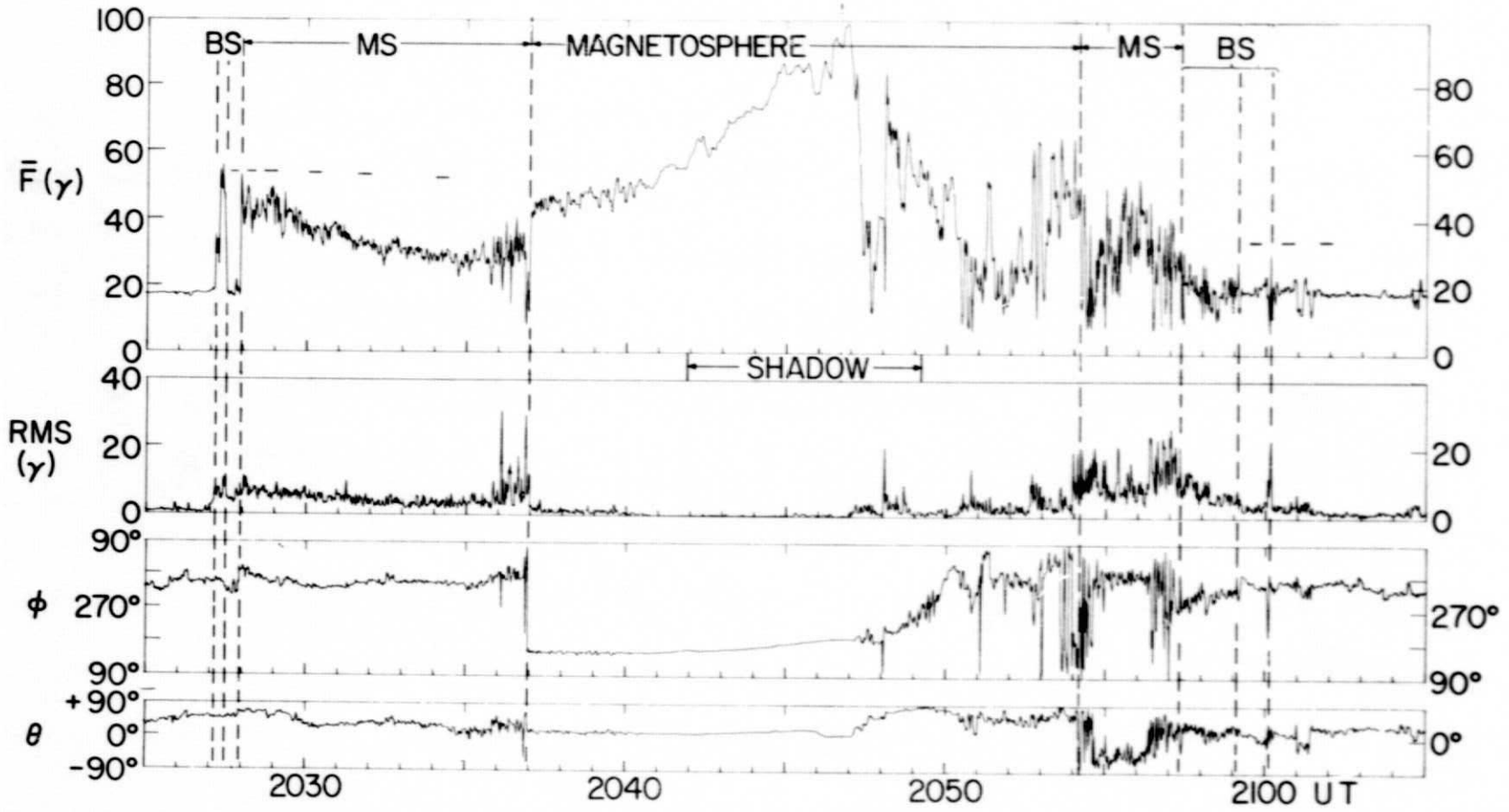

29 MARCH 1974

FIGURE 1

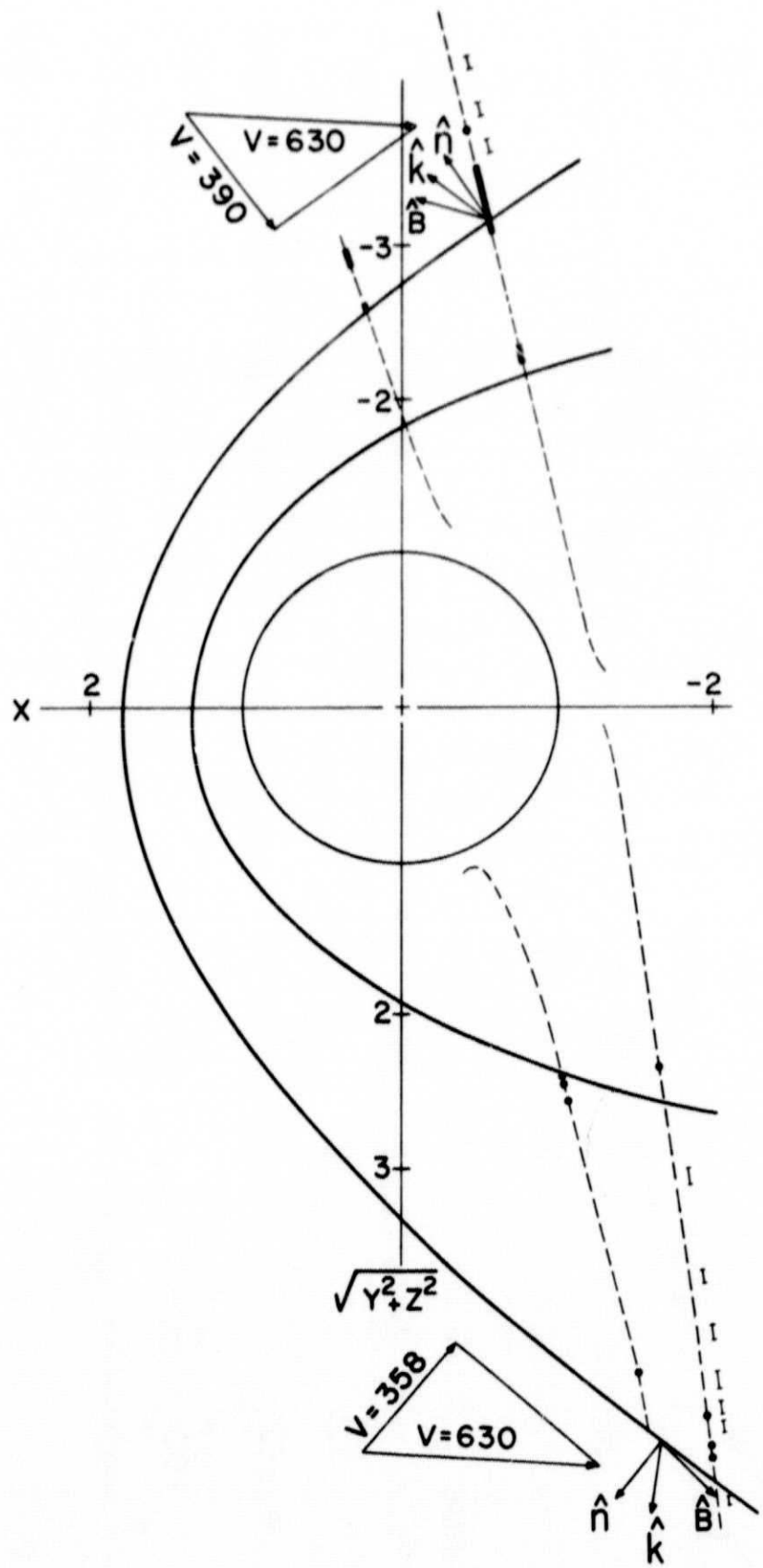

FIGURE 2

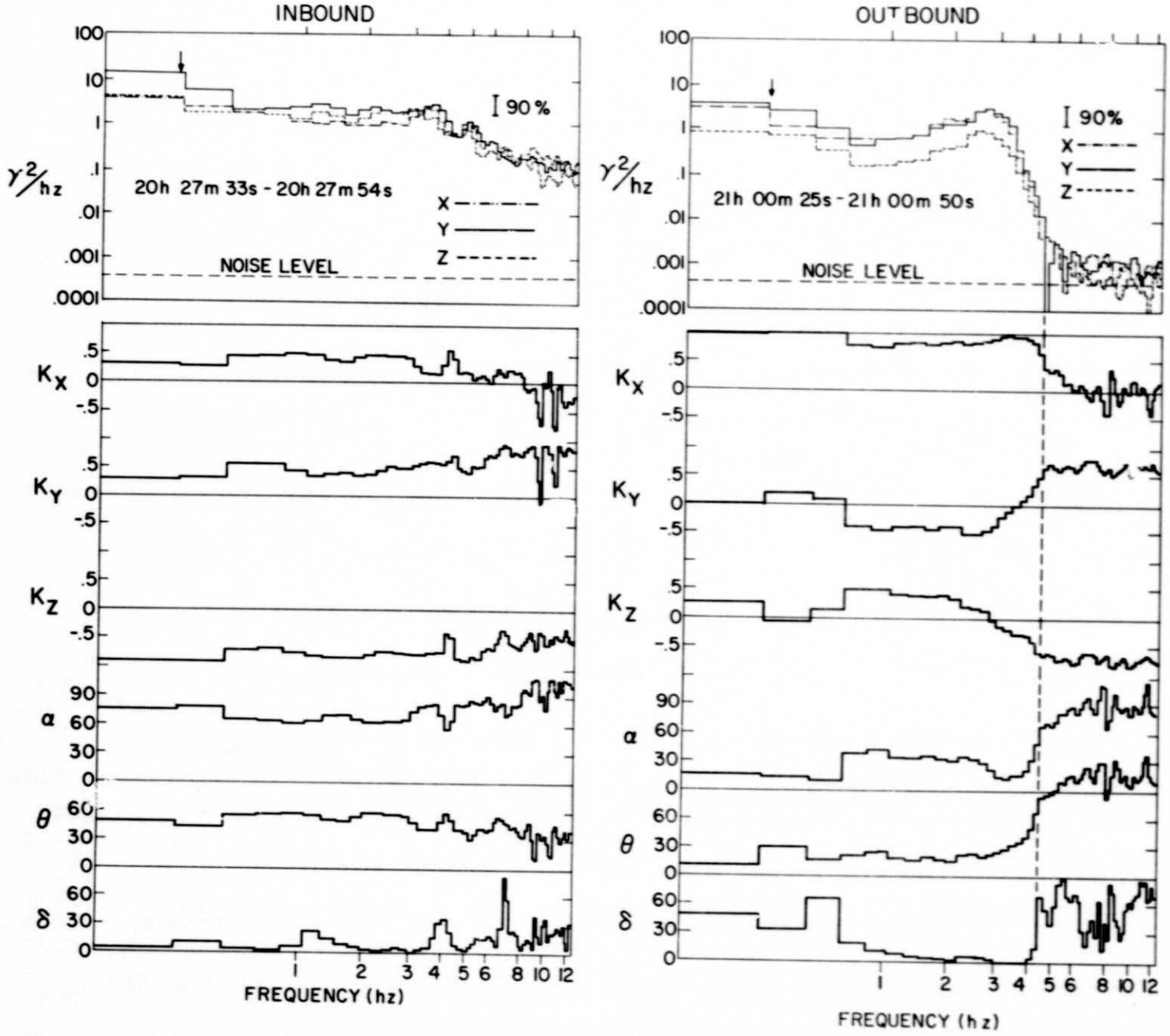
INBOUND
OUTBOUND
100
10
1
.1
.01
.001
.0001
γ²/hz
90%
X
Y
Z
20h 27m 33s - 20h 27m 54s
21h 00m 25s - 21h 00m 50s
NOISE LEVEL
K_X
K_Y
K_Z
.5
0
-.5
α
90
60
30
0
θ
δ
1 2 3 4 5 6 8 10 12
FREQUENCY (hz)

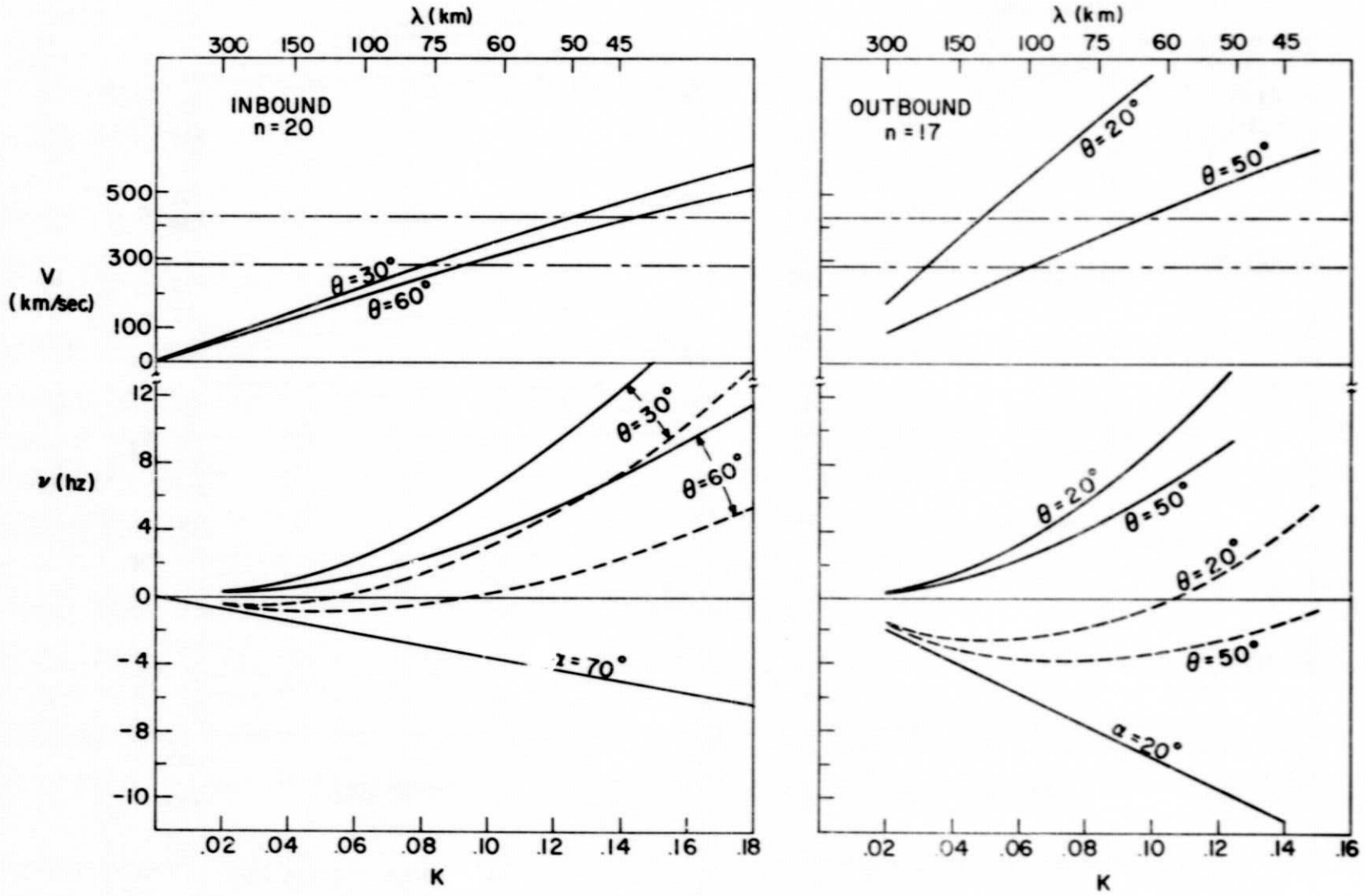
λ (km)
300 150 100 75 60 50 45
INBOUND
n = 20
V
(km/sec)
500
300
100
0
θ=30°
θ=60°
ν (hz)
12
8
4
0
-4
-8
-10
θ=30°
θ=60°
α=70°
.02 .04 .06 .08 .10 .12 .14 .16 .18
K
λ (km)
300 150 100 75 60 50 45
OUTBOUND
n = 17
θ=20°
θ=50°
θ=20°
θ=50°
θ=20°
θ=50°
α=20°
.02 .04 .06 .08 .10 .12 .14 .16
K

FIGURE 4

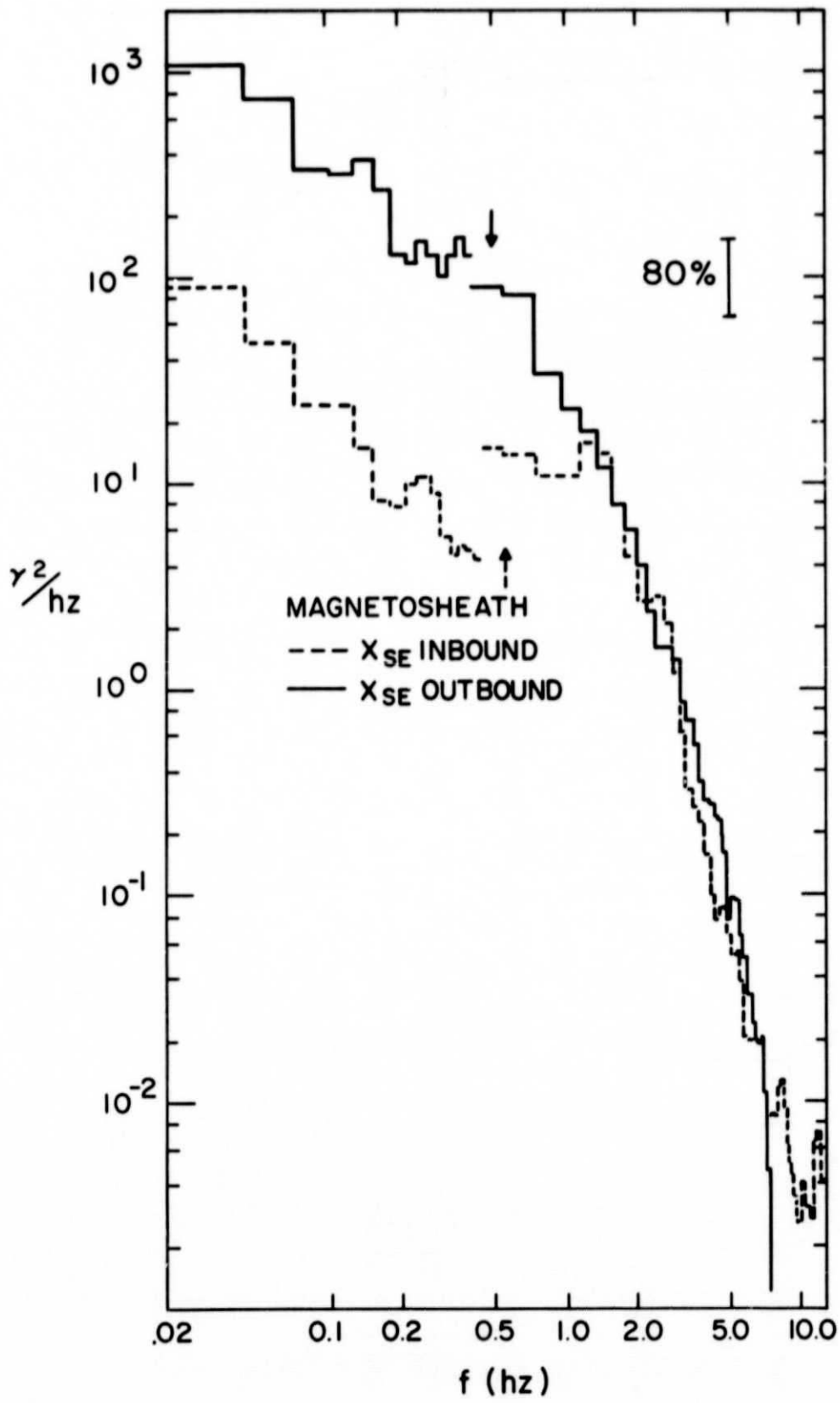
10^3
10^2
10^1
10^0
10^{-1}
10^{-2}
γ^2/hz
80%
MAGNETOSHEATH
--- X_{SE} INBOUND
—— X_{SE} OUTBOUND
.02
0.1
0.2
0.5
1.0
2.0
5.0
10.0
f (hz)

FIGURE 5

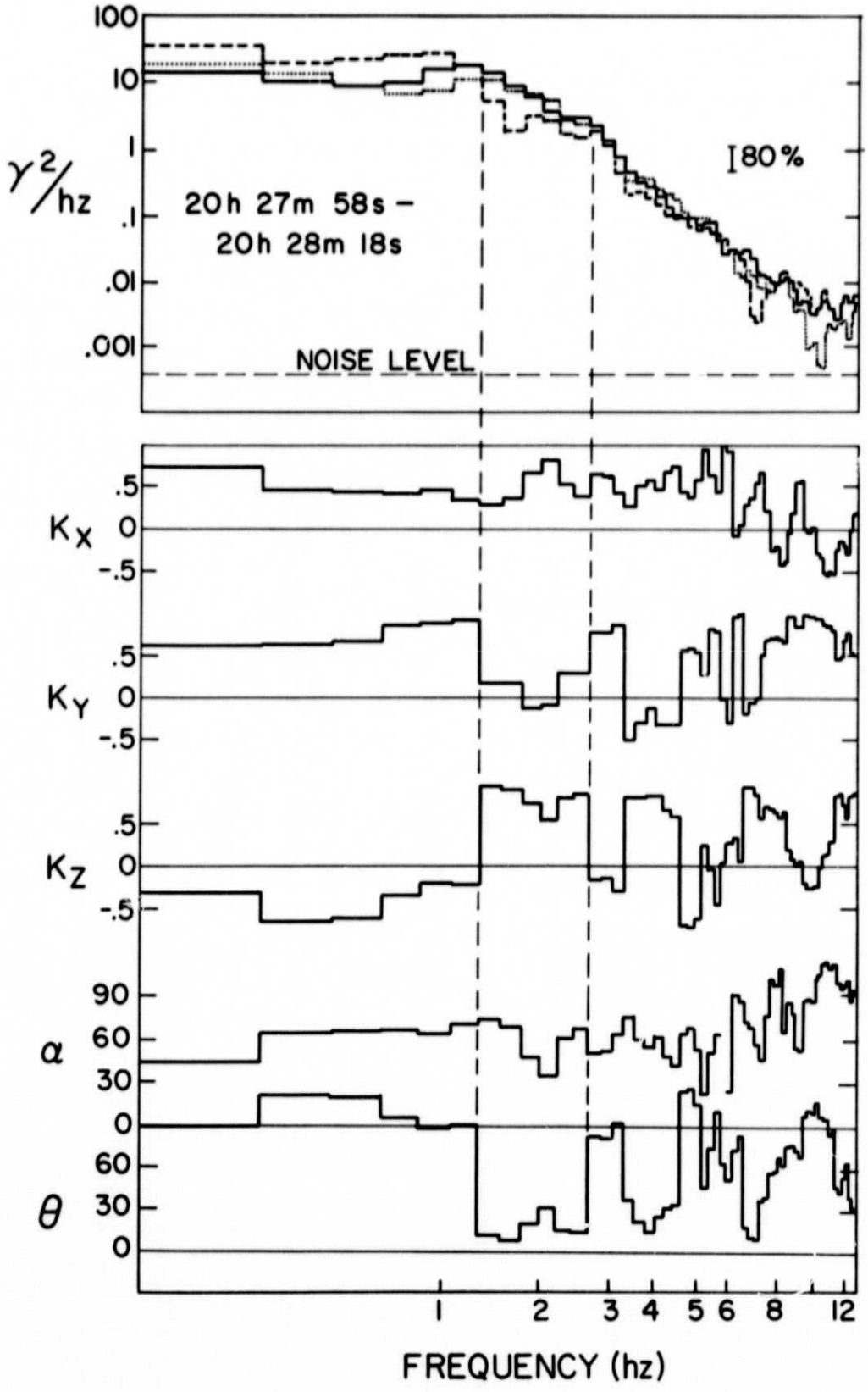
100
10
1
.1
.01
.001
γ²/hz
20h 27m 58s –
20h 28m 18s
180%
NOISE LEVEL
.5
0
-.5
Kx
Ky
Kz
90
60
30
0
α
θ
1
2
3
4
5
6
8
12
FREQUENCY (hz)

FIGURE 6

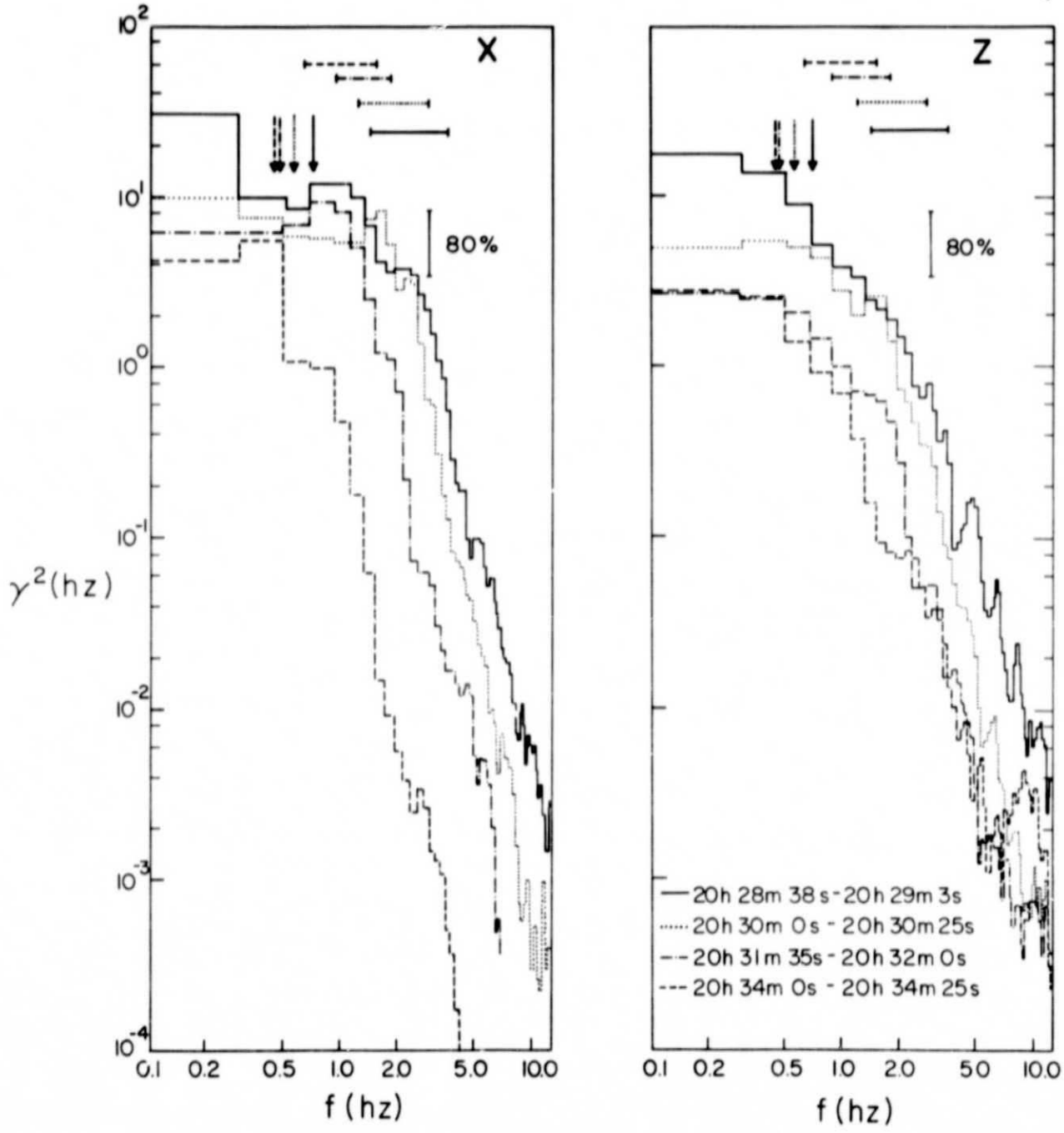
X
Z
80%
80%
γ^2(hz)
f (hz)
f (hz)
20h 28m 38s - 20h 29m 3s
20h 30m 0s - 20h 30m 25s
20h 31m 35s - 20h 32m 0s
20h 34m 0s - 20h 34m 25s

FIGURE 7